Journal of Nuclear Materials 399 (2010) 129–136

Contents lists available at ScienceDirect

Journal of Nuclear Materials

journal homepage: www.elsevier.com/locate/jnucmat

Comparative small-angle neutron scattering study of neutron-irradiated Fe, Fe-based alloys and a pressure vessel steel

F. Bergner [a,*], M. Lambrecht [b], A. Ulbricht [a], A. Almazouzi [b]

[a] Forschungszentrum Dresden-Rossendorf, Institute of Safety Research, P.O. Box 510119, 01314 Dresden, Germany
[b] Nuclear Materials Science Institute, SCK·CEN, Boeretang 200, B-2400 Mol, Belgium

ARTICLE INFO

Article history:
Received 17 July 2008
Accepted 16 November 2009

ABSTRACT

Irradiation-induced damage in reactor pressure vessel steels covers a multitude of different features at the nanometer size scale. The nature, formation kinetics and relative importance of these features are not yet well understood in detail. It also turned out that there is no single experimental technique capable of closing all the remaining gaps. The present approach is based on the idea that significant progress can be achieved by investigating the same set of neutron-irradiated model alloys of increasing complexity with several experimental techniques including transmission electron microscopy (TEM), atom probe tomography (APT), positron annihilation spectroscopy (PAS) and small-angle neutron scattering (SANS). The aim of the effort is to explore both complementarity and overlaps of the information gained from individual techniques and to close gaps by introducing proper models. In the present paper the results obtained by means of SANS are reported, self-consistent interpretation is given and the results are qualified for the discussion in combination with the other experimental techniques to be given in separate papers.

1. Introduction

Knowledge of the detailed nature of nanometer-sized irradiation-induced defect-solute clusters in neutron-irradiated Fe-based alloys and reactor pressure vessel (RPV) steels is of vital importance for models aimed at linking primary neutron damage to the long-term degradation of mechanical properties. There exists an extensive literature about the nature of these features, e.g. [1–11]. However, the overall picture at the nanoscale including types, fractions, morphology and composition of clusters as well as mechanisms of cluster formation is still incomplete. It turned out that there is no individual experimental technique capable of explaining all the aspects in a particular material, e.g. [10]. The results obtained from different techniques even seem to be inconsistent in some cases [11,12], which clearly points to the need of a better understanding.

In order to obtain a more complete picture about the nature of irradiation-induced clusters it is important

- to combine different state-of-the-art experimental techniques, such as transmission electron microscopy (TEM), small-angle neutron scattering (SANS), positron annihilation spectroscopy (PAS) and atom probe tomography (APT), proven to be sensitive to certain details of neutron damage;
- to apply the selected set of experimental techniques to the same set of Fe-based alloys of increasing complexity (from pure Fe to RPV steel) and to expose each of the materials involved to the same set of well-defined irradiation conditions;
- to identify gaps and overlaps among the individual pieces of information gained from the application of different experimental techniques and to fill the gaps using appropriate models calibrated on the basis of experimental results available in the neighborhood of any gap.

An effort based on the kind of approach outlined above was initiated at SCK·CEN, where a set of model alloys was characterized [13,14] and exposed to neutron irradiation at two different dose rates and up to several doses [13,14]. Furthermore, the mechanical property changes due to neutron irradiation were examined as a basis [13–15]. Within the international project REVE [13] and the European project PERFECT [16] the materials were distributed among project partners in order to apply different experimental techniques, to relate the results to each other and to put them into a modeling framework.

In the present contribution SANS experiments are reported and the effects of alloy composition and neutron dose on the SANS results are discussed. It is shown that SANS results comprise rich information including size, concentration and type of clusters and are sensitive to both alloy composition and neutron dose. Furthermore, we observe that SANS results are relevant in the sense of being strongly correlated with irradiation-induced

* Corresponding author. Tel.: +49 351 260 3186; fax: +49 351 260 2205.
E-mail address: f.bergner@fzd.de (F. Bergner).

0022-3115/$ - see front matter © 2009 Elsevier B.V. All rights reserved.
doi:10.1016/j.jnucmat.2009.11.011

mechanical property changes. Both the results of complementary experimental techniques applied to the same set of alloys [17–19] and a comprehensive analysis of the combined results will be given in companion papers.

Flux (dose rate) effects on the microstructure of neutron-irradiated RPV steels and model alloys are an important issue [20–22]. In the work reported here, a relatively high specific value of flux was applied intentionally and flux effects are not considered. However, the materials were also irradiated at a lower level of flux and the findings related to flux effects will be reported in separate papers.

2. Experiments

2.1. Materials and irradiation

Neutron-irradiated materials investigated by means of small-angle neutron scattering (SANS) are listed in Table 1 [13]. A 16MND5 type RPV steel is included. Chemical composition was analyzed by Induced Coupled Plasma Spectroscopy (ICP–MS). The materials were cold worked, annealed at 1073 K for 1 h in argon atmosphere, and subsequently quenched in water. The values of the average grain size and dislocation density determined for the individual alloys are given in Table 2. It is worth noticing that exactly the same samples investigated here were also analyzed by positron annihilation techniques [19,23].

The materials were neutron-irradiated in the Callisto rig (IPS2) in the Belgian reactor (BR2) at Mol [13,14]. An irradiation temperature of 300 °C was maintained. The full set of irradiation conditions is summarized in Table 3. The material conditions studied by means of SANS are summarized in Table 4. It should be noted that the neutron flux is three orders of magnitude higher than the typical flux the pressure vessel of a pressurized water reactor is exposed to.

2.2. Small-angle neutron scattering (SANS)

The SANS experiments were performed at two different experimental facilities. One was carried out at the SANS instrument of the SINQ facility of PSI [24] at a wavelength of 0.5 nm with a sample-detector distance of 2 m. The range of the magnitude of the scattering vector, Q, from 0.3 nm^{-1} to 2.7 nm^{-1} was covered. The other part of the SANS measurements was carried out at the PAXE instrument of the Orphee research reactor at LLB Saclay [25] at a wavelength of 0.6 nm. The SANS intensity was measured with a 2-dimensional 64 cm × 64 cm BF_3-detector. In these experiments the Q-range from 0.16 nm^{-1} to 1.6 nm^{-1} was covered. The samples were placed in a saturation magnetic field. For the analysis including corrections related to both sample holder and detector, absolute calibration as well as separation of magnetic and nuclear contributions of SANS data, we refer to [26]. The incoherent nuclear scattering contribution, $(d\Sigma/d\Omega)_{inc}$, was identified for each of the unirradiated materials assuming the scattering intensity to follow Porod's law (i.e. to be proportional to Q^{-4}) for large Q values. The obtained values, $(d\Sigma/d\Omega)_{inc} = 0.0055\ cm^{-1}$ for Fe-alloys and $(d\Sigma/d\Omega)_{inc} = 0.0076\ cm^{-1}$ for the RPV steel, was subtracted from the measured total and nuclear intensities in order to obtain the coherent scattering cross-sections, $(d\Sigma/d\Omega)_c$, we are interested in.

In order to calculate the size distribution of scatterers, a dilute two-phase matrix-inclusion microstructure composed of homogeneous non-magnetic spherical scatterers randomly dispersed in a pure Fe matrix is assumed. For a number of N homogeneous spherical scatterers of radius, R, in the probed volume, V_p, the coherent scattering cross-section $(d\Sigma/d\Omega)_c$ can be expressed as:

$$\left(\frac{d\Sigma}{d\Omega}\right)_C(Q) = \frac{N}{V_p}\Delta\eta^2 V^2(R)|F(Q,R)|^2 \quad (1)$$

$$|F(Q,R)|^2 = \frac{9(\sin QR - QR\cos QR)^2}{(QR)^6} \quad (2)$$

with the volume, V, of the sphere, the magnitude of the scattering vector, Q, and the form factor, F. Magnetic and nuclear scattering are not distinguished in Eq. (1). The scattering contrast, $\Delta\eta^2$, is given by:

$$\Delta\eta_i^2 = \left[(n\bar{b}_i)_S - (n\bar{b}_i)_M\right]^2 \quad (3)$$

where $i = m$ for magnetic scattering and $i = n$ for nuclear scattering. Subscripts S and M refer to scatterer and matrix, respectively, and $\bar{b}_m$ and $\bar{b}_n$ denote the average scattering length for magnetic and nuclear scattering, respectively. In the case of non-magnetic scatterers ($\bar{b}_{m,S} = 0$) in a pure Fe matrix:

$$\Delta\eta_m^2 = (n_{Fe}b_{m,Fe})^2 \quad (4)$$

The indirect transformation method [27], which is based on a description of the size distribution according to Eqs. (1)–(4), was applied to obtain the size distribution of scatterers without assuming a certain type of distribution.

Table 1
Neutron-irradiated materials of the REVE experiment.

Material	Code	Nominal composition (wt.%)
Pure Fe	A	<30 ppm C
Fe–0.1%Cu	C	0.1 Cu (<30 ppm C)
Fe–0.3%Cu	D	0.3 Cu (<30 ppm C)
Fe–Mn–Ni	E	1.2 Mn, 0.7 Ni (<30 ppm C)
Fe–Mn–Ni–Cu	F	1.2 Mn, 0.7 Ni, 0.1 Cu (<30 ppm C)
RPV steel 16MND5	G	0.135 C, 0.009 S, 0.013 P, 0.04 Si, 0.37 Mn, 0.69 Ni, 0.13 Cr, 0.52 Mo, 0.065 Cu

Table 2
Average grain size and dislocation density of the model alloys.

Material	Average grain size/μm	Dislocation density/10^{13} m^{-2}
Pure Fe	250	7
Fe–0.1%Cu	125	9
Fe–0.3%Cu	177	9
Fe–Mn–Ni	88	3.2
Fe–Mn–Ni–Cu	88	3.8

Table 3
Summary of irradiation conditions (Irradiation temperature 300 °C).

Damage dose (dpa)	Neutron fluence (n/m^2)	Neutron flux ($E > 1$ MeV) 1.6×10^{16} n/m^2 s	($E > 1$ MeV) 0.95×10^{18} n/m^2 s
0.026	1.7×10^{23}	–	×
0.032	2.1×10^{23}	×	–
0.051	3.5×10^{23}	–	×
0.10	6.9×10^{23}	–	×
0.19	1.3×10^{24}	–	×

Table 4
Summary of the material conditions studied by SANS.

Neutron flux ($E > 1$ MeV): 0.95×10^{18} n/m^2s					
Material	Code	0.026 dpa	0.051 dpa	0.10 dpa	0.19 dpa
Pure Fe	A	–	–	–	HA42
Fe–0.1%Cu	C	HC12	HC22	HC32	HC42
Fe–0.3%Cu	D	HD12	HD22	HD32	HD42
Fe–Mn–Ni	E	–	HE22	HE32	HE42
Fe–Mn–Ni–Cu	F	–	HF22	HF32	HF42
RPV steel	G	–	HG22	HG32	HG42

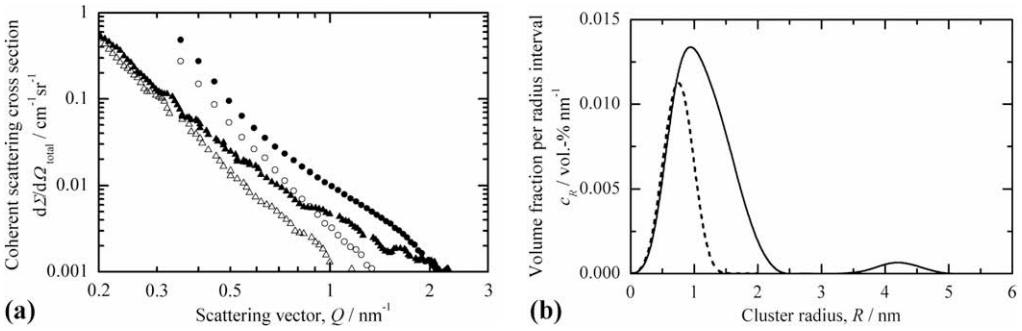

Fig. 1. (a) Total coherent SANS cross-section for pure Fe exposed to doses of 0.19 dpa (full circles) and 0.038 dpa (full triangles), unirradiated references marked as open symbols, (b) Size distribution of irradiation-induced defect clusters calculated for pure Fe exposed to 0.19 dpa (solid line) and to 0.038 dpa (dashed line) [29,30].

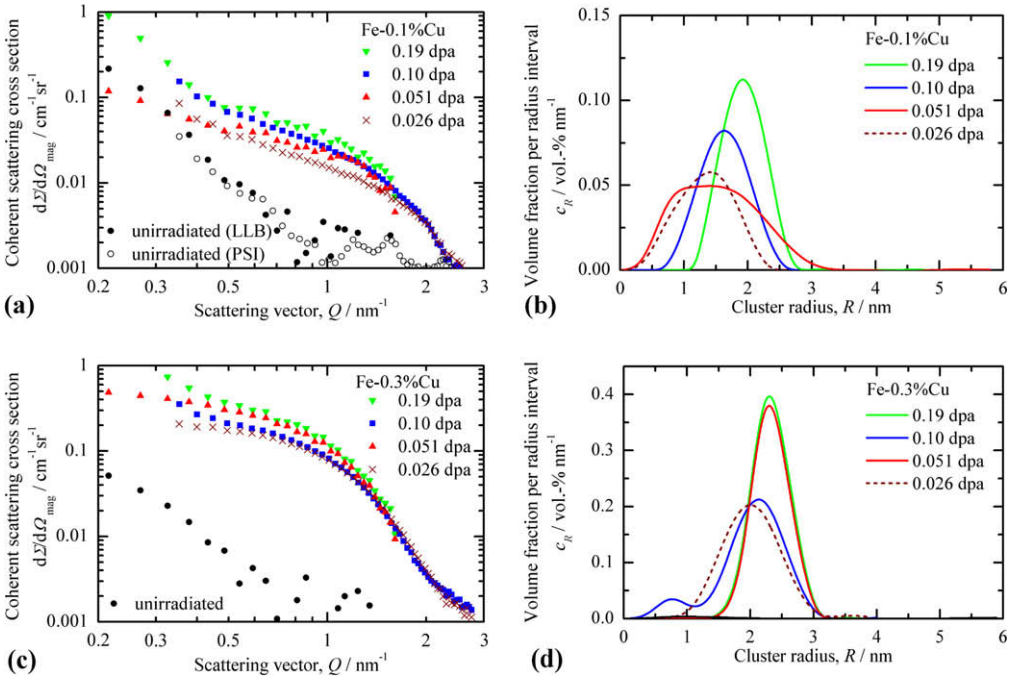

Fig. 2. Magnetic scattering cross-section (a), (c) and size distributions of irradiation-induced scatterers (b), (d) for binary Fe–Cu alloys.

$$\frac{d\Sigma}{d\Omega}(Q) \rightarrow c_R \Delta\eta^2(R) \tag{5}$$

To this end a number of 40 cubic splines with nodes uniformly distributed in the radius range from 0 to 15 nm were specified by means of a weighted least squares procedure in the present case. For each material the unirradiated control was subtracted after performing the transformation.

As long as the magnetic or nuclear scattering contrast, $\Delta\eta^2$, is unknown, the size distribution, c_R, can be obtained in relative units only according to Eq. (5). However, non-magnetic scatterers were preliminarily assumed for the purpose of the presentation of results. In this case the magnetic contrast, $\Delta\eta_m^2$, is known and the calculated size distributions can be obtained in absolute units:

$$c_R = \frac{(c_R \Delta\eta^2)_{m,\text{measured}}}{\Delta\eta_m^2} \tag{6}$$

In the case of non-zero magnetic moment of the scatterers (for instance, if the scatterers contain a significant amount of Fe atoms bearing a magnetic moment), the calculated size distributions represent a lower bound of the real distribution.

The A-ratio originally defined as ratio of the scattering cross-sections, $d\Sigma/d\Omega$, perpendicular and parallel to the magnetic field direction [28] was calculated according to Eq. (7) from the measured size distributions, c_R, of irradiation-induced scatterers scaled with the (a priori unknown) magnetic and nuclear scattering contrast, $\Delta\eta_m^2$ and $\Delta\eta_n^2$, respectively. In general, the magnetic and nuclear scattering contrasts are different functions of radius, R. In order to obtain a robust average value of the A-ratio, the size distributions were integrated over R.

$$A = \frac{(d\Sigma/d\Omega)_\perp}{(d\Sigma/d\Omega)_\parallel} = \frac{(d\Sigma/d\Omega)_m}{(d\Sigma/d\Omega)_n} + 1 = \frac{\int (c_R \Delta\eta^2)_{m,\text{measured}} dR}{\int (c_R \Delta\eta^2)_{n,\text{measured}} dR} + 1 \tag{7}$$

3. Results

The total coherent scattering cross-section obtained for pure Fe [29,30] is presented in Fig. 1. In the case of pure Fe, the magnetic scattering cross-section was determined in order to check, if the calculated average A-ratio corresponds to what theory predicts for vacancy-type clusters (A = 1.4). As this was confirmed, the size

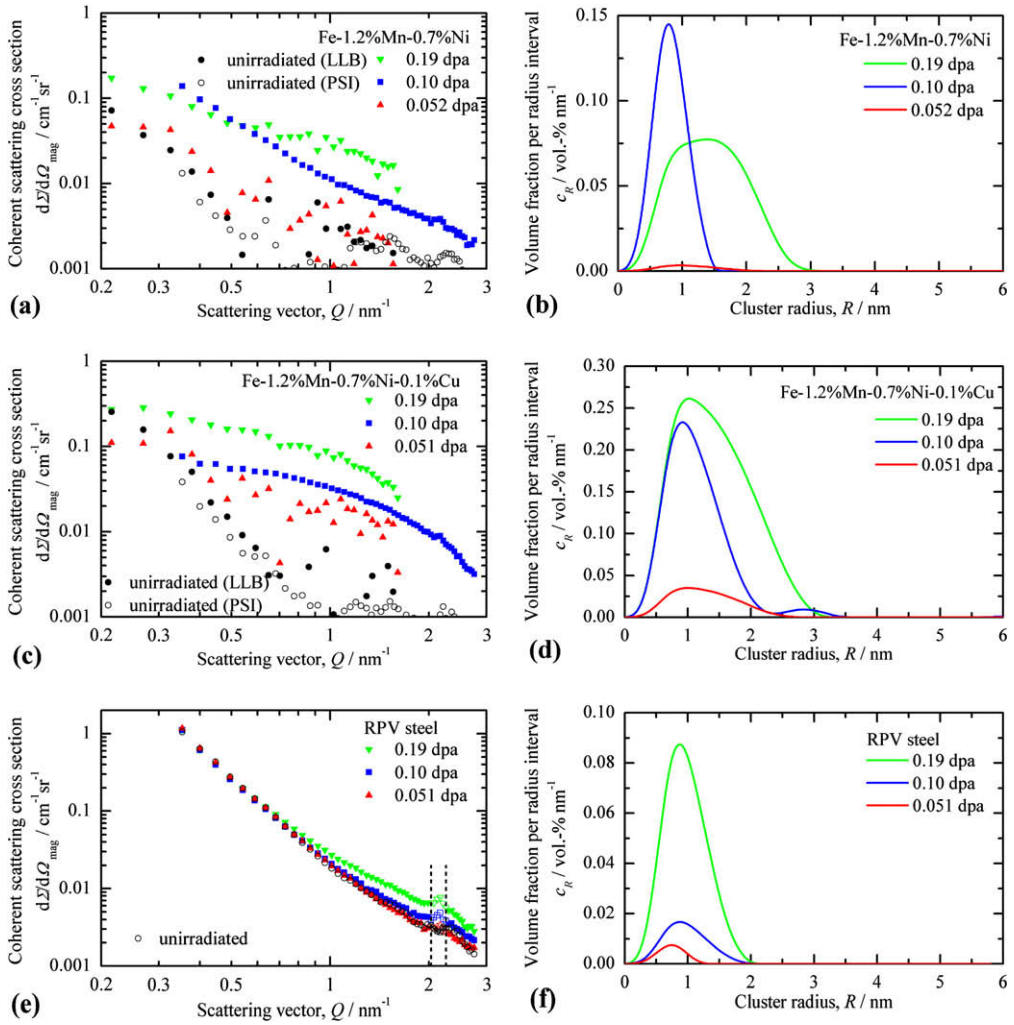

Fig. 3. Magnetic scattering cross-section (a), (c), (e) and size distributions of irradiation-induced scatterers (b), (d), (f) for complex alloys (a)–(d) and 16MND5 type RPV steel (e), (f).

distribution of scatterers can be calculated from the nuclear scattering cross-section. The result obtained for the size distribution is presented in Fig. 1b. The result for another heat of pure Fe irradiated under similar conditions is shown for comparison [29,30].

In all the other cases, the size distributions were calculated from the magnetic scattering cross-sections on the assumption of non-magnetic scatterers (magnetic holes in a ferromagnetic matrix). The results are compiled in Figs. 2 and 3. In Fig. 3e there seems to be an experimental artefact (in between the dashed lines). As the indicated small intermediate Q-range is not required for the reconstruction of the size distribution, the corresponding values of the scattering cross-section were ignored in the further analysis. It is important to note that the lower detection limit of SANS is about 0.5 nm in terms of radius. Any modification of the shape of the reconstructed size distributions at sizes below the detection limit would have no effect on the scattering curves and cannot be ruled out.

We have observed that the size distributions of irradiation-induced scatterers are essentially single peaked. The results obtained for the peak radius, the total volume fraction of scatterers, their total number density and the A-ratio are summarized in Table 5 for all investigated materials. The volume fraction is a measure of the integral over the obtained size distributions. Both, total volume fraction and number density were calculated using the assumption that all the present scatterers are of non-magnetic character and represent lower bounds for all cases, where scatterers bear a non-zero magnetic moment. The calculated total volume fraction is independent of the shape of the scatterers. Peak radius and A-ratio are valid independently of the assumption on the magnetic character of the scatterers. These quantities represent effective values for non-spherical or graded scatterers. The yield stress increase is given in Table 5 for comparison.

4. Discussion

4.1. Mechanical property correlation

According to former experience there is a pronounced correlation between the square root of volume fraction of irradiation-induced clusters and either yield stress increase or hardness increase [31,32]. We remind that the SANS volume fraction was calculated on the assumption of non-magnetic clusters. In order to check this type of correlation in the present case, the complete set of data pairs was included in the scatter plot, Fig. 4, without distinguishing particular materials. Fig. 4 shows that a pronounced correlation is confirmed in spite of the diversity of both the alloys involved and the nature of the irradiation-induced features formed. First, this finding additionally confirms the general correctness of the complex procedure of data analysis including

Table 5
Summary of SANS results and irradiation-induced yield stress increase.

Material	Neutron dose/dpa	Peak radius/nm	*A*-ratio	Volume fraction/%	Number density/10^{22} m^{-3}	Yield stress increase/MPa
Pure Fe	0.19	0.95	1.4	0.014	4	127
Fe–0.1%Cu	0.026	1.4	1.4	0.069	12	132
	0.051	1.4	>10	0.083	14	143
	0.10	1.6	4.6	0.083	7	205
	0.19	1.9	2.6	0.089	4	188
Fe–0.3%Cu	0.026	2.0	2.5	0.229	9	210
	0.051	2.3	9	0.280	5	210
	0.10	2.1	7	0.237	15	254
	0.19	2.3	2.4	0.300	5	236
Fe–Mn–Ni	0.051	0.9	1.1	0.003	0.9	71
	0.10	0.8	1.3	0.09	38	125
	0.19	1.4	1.6	0.13	21	194
Fe–Mn–Ni–Cu	0.051	1.0	1.2	0.046	10	167
	0.10	0.95	1.9	0.25	66	226
	0.19	1.05	2.0	0.41	77	300
RPV steel	0.051	0.75	1.5	0.005	2	62
	0.10	0.85	1.4	0.015	5	116
	0.19	0.85	2.1	0.08	24	155

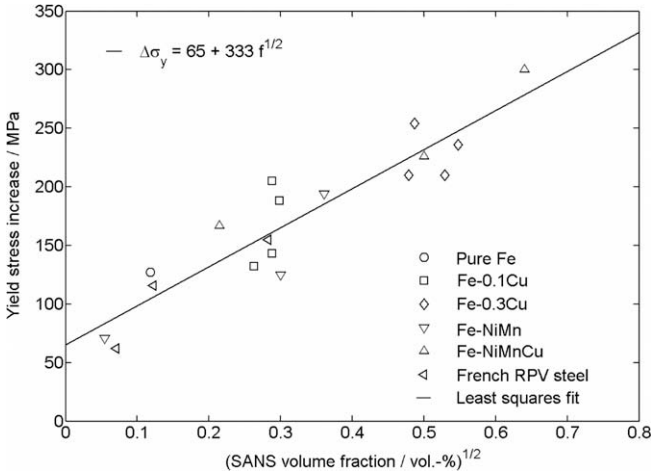

Fig. 4. Correlation between square root of volume fraction and yield stress increase with each of the alloys and irradiation conditions of this work involved.

absolute calibrations and corrections, separation of magnetic and nuclear contributions, subtraction of incoherent scattering as well as the applicability of the assumptions made. Second, our finding shows that the volume fraction of irradiation-induced clusters derived from SANS data is relevant in the sense that the observed clusters themselves are either responsible for the irradiation-induced hardening or correlated with the features responsible for hardening. The straight line fitted to the data points in Fig. 4 indicates that there are essentially two components of the yield stress increase. One component is linearly related to the square root of cluster volume fraction. The second one given by the intersection with the ordinate is not related with volume fraction. This part can be ascribed to features of size below the detection limit of SANS (0.5 nm in radius) and/or of scattering contrast too small to give rise to detectable scattering (e.g. dislocation loops).

4.2. Pure Fe

SANS results for pure Fe are available for a dose of 0.19 dpa (Table 5). The measured *A*-ratio of 1.4 agrees with the value calculated for vacancy-type clusters on the basis of Eqs. (3) and (7) (ignoring the subscript "measured" and reducing the fraction in Eq. (7) [32]). In order to get a first impression on the effect of dose, the results can be compared with a SANS measurement performed for another heat of pure Fe neutron-irradiated up to a dose of 0.038 dpa [29,30] (Table 6). The comparison indicates that both peak radius of vacancy clusters and number density are slightly increasing functions of dose. The effect of dose on the volume fraction is a consequence of the latter two effects. The combination of both effects gives an increase weaker than a linear one.

Carefull examination of the scattering curves (Fig. 1) indicates that there is a systematic *Q*-independent irradiation-induced increase of the scattering cross-section at low values of *Q* for both heats of pure Fe. In [30] it was checked that this increase is definitely not caused by the population of planar dislocation loops detected by means of TEM. Rather, a distribution of nanovoids of diameters up to about 20 nm to be described in a companion paper focussed on TEM [17] does explain the observed increase of the scattering cross-section.

4.3. Fe–Cu

The total volume fraction of irradiation-induced clusters, the peak radius and the *A*-ratio are presented in Fig. 5a–c, respectively, as a function of dose. We have observed that the volume fraction of clusters derived from the SANS results exhibits a saturation-like behaviour and that the saturation values almost coincide with the atomic Cu fractions of the binary Fe–0.1%Cu (0.088 at.%) and Fe–0.3%Cu (0.26 at.%) (see Table 5 and Fig. 5a). The slightly reduced volume fractions for a dose of 0.026 dpa indicate that the saturation level was just approached at about this dose.

The estimated peak size is a slightly increasing function of dose for Fe–0.1%Cu. For Fe–0.3%Cu the peak size is generally larger but no dose dependence (Fig. 5b) could be noticed. The number density for Fe–0.1%Cu tends to decrease mainly as a result of increasing size at constant volume fraction.

The measured values of the *A*-ratio of both types of Fe–Cu alloys follow similar dose dependences (Fig. 5c). They are bounded by the *A*-ratios expected for pure fully coherent Cu precipitates, $A = 12$, and for pure vacancy clusters, $A = 1.4$ [32]. There is a monotonic relationship between *A*-ratio and Cu-vacancy ratio of a Cu-vacancy cluster (Fig. 6) [32,33]. The dose dependences of the *A*-ratio and, therefore, of the Cu-vacancy ratio of the average cluster pass through a maximum at about 0.05 dpa.

The peak in the dose dependence of the *A*-ratio can be explained tentatively on the basis of the following reasoning: The steady-state concentration of vacancies under irradiation is a decreasing function of the concentration of vacancy sinks and traps. At an early stage of cluster evolution there are few small Cu-clusters

Table 6
Comparison with results obtained for a different lot of pure Fe [29,30].

Dose/dpa	Peak radius/nm	*A*-ratio	Volume fraction/%	Number density/m^{-3}
0.19	0.95	1.4	0.014	4×10^{22}
0.038	0.78	1.4	0.006	3×10^{22}

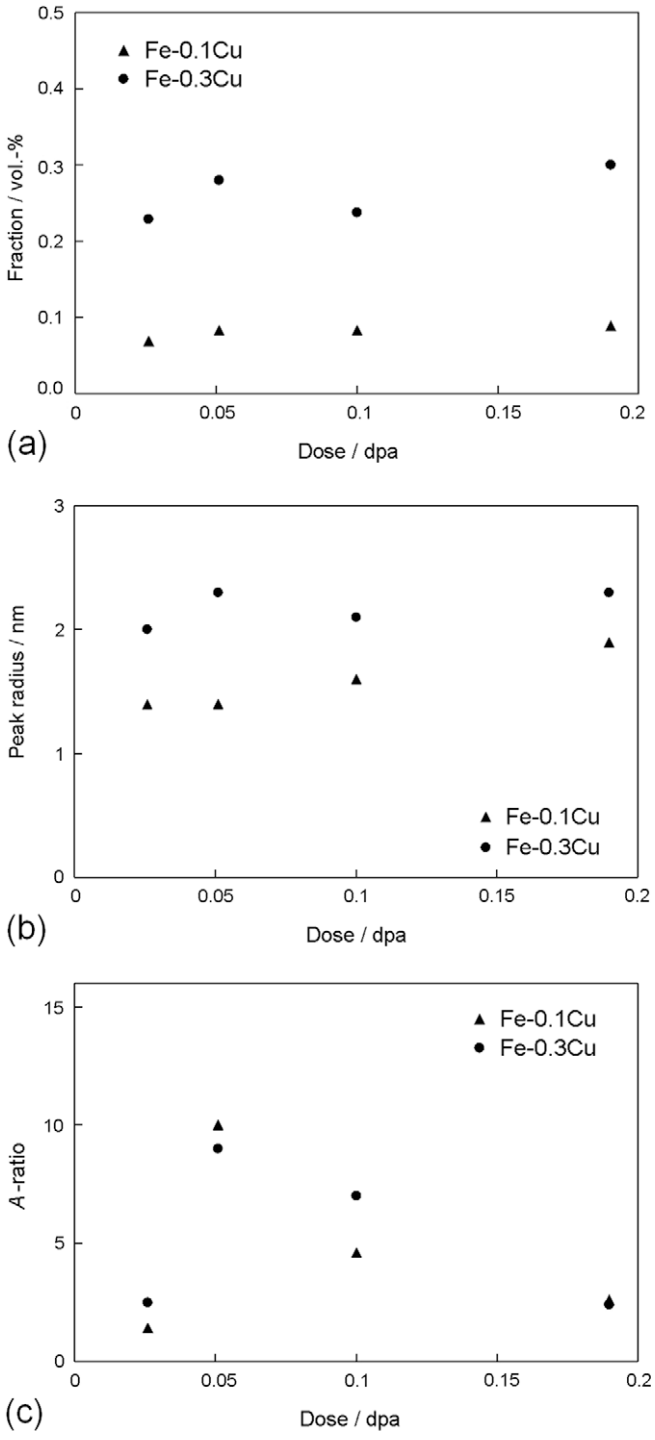

Fig. 5. Dose dependence of total volume fraction (a), peak radius (b) and *A*-ratio (c) of irradiation-induced clusters in binary Fe–Cu alloys.

operating as vacancy traps, the steady-state vacancy concentration is high and the existing Cu-clusters absorb a high fraction of vacancies. At a later stage a higher concentration of larger mixed

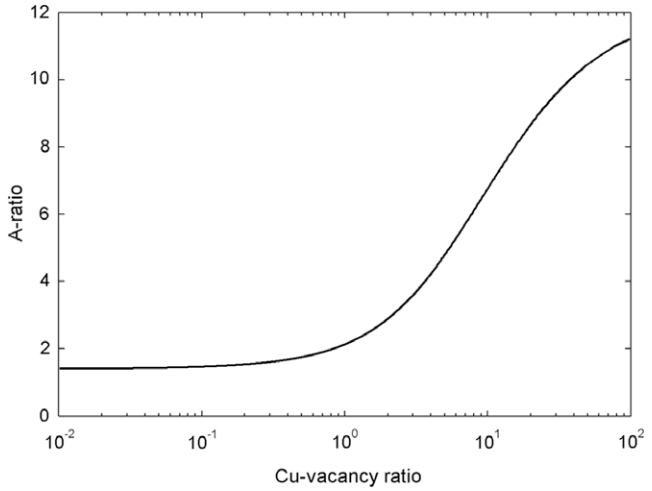

Fig. 6. Relationship between the Cu-vacancy ratio of a Cu-vacancy cluster in Fe and the *A*-ratio.

vacancy-Cu-clusters has formed causing the concentration of vacancy traps to increase and the steady-state vacancy concentration to decrease. At this stage the Cu fraction in the mixed clusters increases giving rise to the observed increase of the *A*-ratio. Still later the matrix is depleted of Cu atoms. No further Cu atoms can be absorbed by the clusters but vacancies are still available giving rise to a decrease of the *A*-ratio and finally to the formation of a peak in the dependence of the *A*-ratio on time or dose at constant dose rate.

It should be noticed that an increasing Cu-vacancy ratio (or increasing *A*-ratio) is consistent with a sequence deduced from a combined investigation using APT and rate theory and described as heterogeneous nucleation of Cu at preexisting vacancy clusters [34,35]. On the other hand, a decreasing Cu-vacancy ratio (or decreasing *A*-ratio) is compatible with the generation of microvoids at preexisting Cu-clusters as deduced from a combination of PAS and rate theory [36,14]. The present investigation indicates a crossover in the evolution of the Cu-vacancy ratio. The analysis of the same alloys with PAS techniques combining positron lifetime measurement and coincidence Doppler broadening has shown the same effect [19,23].

Fe atoms in the clusters bearing the same magnetic moment as matrix Fe do not influence the *A*-ratio. However, the magnetic moment of Fe depends on the Cu/Fe ratio in the clusters. Therefore, changes of this ratio as a function of dose might also contribute to the dose dependence of the *A*-ratio [25].

4.4. Fe–Mn–Ni and Fe–Mn–Ni–Cu

For both alloys a slight increase of the *A*-ratio of irradiation-induced clusters with dose is observed. The *A*-ratio obtained for Fe–Mn–Ni is much smaller than for the Fe–Cu alloys and, at least at the lower doses, even smaller than for pure Fe ($A = 1.4$). This can only be explained with the negative nuclear scattering length of Mn and implies that Mn atoms are an important constituent of the irradiation-induced defect-solute clusters. This result indicates irradiation-induced clustering as opposed to irradiation-enhanced precipitation to occur, because the Mn content is below the solubility limit of Mn in Fe of about 5 at.%. A similar observation was reported in [30] for irradiation-induced clustering of Ni in a binary Fe–3%Ni alloy. The *A*-ratio obtained for Fe–Mn–Ni–Cu is still much smaller than for Fe–0.1%Cu (Mn effect) but larger than for Fe–Mn–Ni (Cu effect). It is also interesting to note that the *A*-ratio found for Fe–Mn–Ni is less than the value observed in our previous investigation for Fe–Mn-Si ($A = 1.7$) [33].

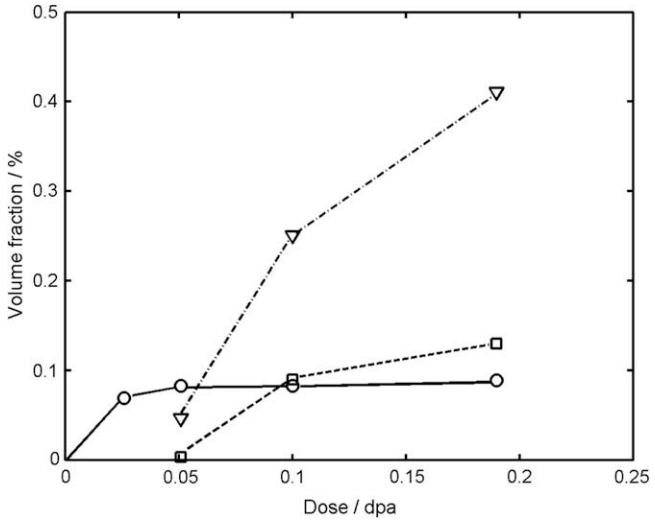

Fig. 7. Dose dependence of the volume fraction of irradiation-induced defect-solute clusters for Fe–0.1%Cu (circles), Fe–Mn–Ni (squares) and Fe–Mn–Ni–0.1%Cu (triangles).

Table 7
Comparison of the sum of volume fractions for Fe–0.1%Cu and Fe–Mn–Ni with the volume fraction measured for Fe–Mn–Ni–0.1%Cu.

Dose/dpa	Fe–0.1%Cu + Fe–Mn–Ni	Fe–Mn–Ni–0.1%Cu
0.051	0.086	0.046
0.10	0.173	0.25
0.19	0.219	0.41

For both Fe–Mn–Ni and Fe–Mn–Ni–Cu there is no clear dose dependence of the peak radius. Cluster size is found to be smaller than for Fe–Cu alloys and similar as for pure Fe.

A pronounced increase of the volume fraction of defect-solute clusters with dose is observed for both alloys without any indication of a saturation-like behaviour (Fig. 7). A similar behaviour has been observed in the yield stress increase with irradiation dose. At higher doses, 0.10 dpa and 0.19 dpa, the cluster volume fraction is significantly larger than the sum of the fractions for Fe–0.1%Cu and Fe–Mn–Ni (Table 7). This shows that the effect of Mn and/or Ni synergistically combines with the effect of Cu.

4.5. RPV steel

The peak radius observed for the RPV steel is the smallest one of the alloys investigated. There is no significant dependence on dose. The volume fraction of the irradiation-induced defect-solute clusters exhibits a pronounced, monotonically increasing dose dependence. From the viewpoint of composition (Table 1), the RPV steel should be best comparable with Fe–Mn–Ni–Cu and Fe–Mn–Ni. Indeed, the Ni contents agree for each of the three materials and the Cu content of the RPV steel is in between the two others. However, for doses of 0.10 dpa and 0.19 dpa the volume fraction for the RPV steel is observed to be less than both, not in between. This observation may be due either to direct participation of Mn, the content of which is much less for the RPV steel, or to indirect effects of other elements (e.g. carbon) on cluster formation.

5. Conclusions

Neutron-irradiated pure Fe, Fe–0.1%Cu, Fe–0.3%Cu, Fe–NiMn, Fe–NiMnCu and a 16MND5 type RPV steel were investigated by means of SANS. The following conclusions on the nature of irradiation-induced clusters including the effects of neutron dose and composition can be drawn on the basis of the extracted SANS results:

(1) For pure Fe irradiation-induced defect clusters are detected by SANS. The measured *A*-ratio of 1.4 agrees with the expectation for vacancy-type clusters.
(2) For Fe–Cu alloys the dose dependence of the volume fraction of irradiation-induced defect-solute clusters exhibits an initial increase followed by a saturation-like behaviour. The volume fraction at saturation approximately coincides with the atomic fraction of Cu in both types of Fe–Cu alloy. The dose dependence of the *A*-ratio passes through a peak at about 0.051 dpa. A tentative explanation for the peak proposed in the discussion is based on the relation between *A*-ratio and Cu-vacancy ratio in the average cluster. According to this interpretation the peak marks the instant of time during irradiation, at which Cu depletion of the matrix is completed.
(3) For Fe–Mn–Ni and Fe–Mn–Ni–Cu the volume fraction of irradiation-induced defect-solute clusters is observed to increase monotonically with dose. The volume fraction for Fe–Mn–Ni–Cu increases faster than the sum of those for Fe–0.1%Cu and Fe–Mn–Ni indicating a synergistic effect of Mn and/or Ni with Cu. The observed values of the *A*-ratio less than 1.4 shows that Mn is an important constituent of the clusters.
(4) For the RPV steel the volume fraction of irradiation-induced defect-solute clusters also increases monotonically with dose, but the increase is found to be slower than expected from the Ni and Cu contents. Possible explanations are related to the lesser Mn content in the RPV steel or to the indirect effect of other alloying elements.

A fairly strong correlation between the square root of volume fraction of irradiation-induced clusters observed by means of SANS and the irradiation-induced increase of yield strength was found.

The intention of the microstructural investigation of the materials involved in this work was to combine the results of different methods including ATP, PAS, TEM and SANS. The presented results are a contribution to this effort. The combination of methods will be vital for the final clarification of the nature and formation kinetics of irradiation-induced features. The results are a proper basis for the validation of models describing the long-term evolution of cluster populations. Finally, it should be borne in mind that transfer of the present results to reactor operation conditions requires the consideration of flux effects.

Acknowledgements

This work was supported within the European Integrated Project PERFECT under Contract no. F6O-CT-2003-508840. One of the authors (AA) would like to thank Drs J. Kohlbrecher and M. Grosse (PSI) and M.-H. Mathon (LLB) for their assistance and professionalism during the performance of the SANS measurements.

References

[1] F. Frisius, R. Kampmann, P.A. Beaven, R. Wagner, Dimensional Stability and Mechanical Behavior of Irradiated Metals and Alloys-VI, BNES, London, 1983. p. 171.
[2] J.T. Buswell, C.A. English, M.G. Hetherington, W.J. Phythian, G.D.W. Smith, G.M. Worrall, ASTM STP 1046, American Society for Testing and Materials, Philadelphia, PA, 1990. p. 127.
[3] G. Brauer, F. Eichhorn, F. Frisius, R. Kampmann, in: Effects of Radiation on Materials: 16th International Symposium, ASTM STP 1175, American Society for Testing and Materials, Philadelphia, PA, 1993, p. 503.

[4] G.R. Odette, in: Materials Research Society Symposium Proceedings, vol. 373, Materials Research Society, Warrendale, Pennsylvania, 1995, p. 137.
[5] T.J. Williams, W.J. Phythian, ASTM STP1270, American Society for Testing and Materials, West Conshohocken, PA, 1996. p. 191.
[6] P. Pareige, K.F. Russel, R.E. Stoller, M.K. Miller, J. Nucl. Mater. 250 (1997) 176–183.
[7] G.R. Odette, B.D. Wirth, J. Nucl. Mater. 251 (1997) 157–171.
[8] G.R. Odette, G.E. Lucas, Radiat. Eff. Defects Solids 144 (1998) 189–231.
[9] S.C. Glade, B.D. Wirth, G.R. Odette, P. Asoka-Kumar, P.A. Sterne, R.H. Howell, Philos. Mag. 85 (2005) 629–639.
[10] R.G. Carter, N. Soneda, K. Dohi, J.M. Hyde, C.A. English, W.L. Server, J. Nucl. Mater. 298 (2001) 211–224.
[11] M.K. Miller, B.D. Wirth, G.R. Odette, Mater. Sci. Eng A353 (2003) 133–139.
[12] A. Ulbricht, F. Bergner, J. Böhmert, M. Valo, M.-H. Mathon, A. Heinemann, Philos. Mag. 87 (2007) 1855–1870.
[13] L. Malerba, E. van Walle, C. Domain, S. Jumel, J.-C. van Duysen, in: Proceedings of ICONE 10: 10th International Conference on Nuclear Engineering, ASME, Arlington (VA), USA, 2002 (paper 22260).
[14] K. Verheyen, M. Jardin, A. Almazouzi, J. Nucl. Mater. 351 (2006) 209–215.
[15] M. Lambrecht, A. Almazouzi, The influence of different chemical elements in the hardening embrittlement of RPV steels, OECD Handbook: Nuclear Science "Structural Materials for Innovative Nuclear Systems (SMINS)", 2008, pp. 457–466.
[16] D. Lidbury, S. Bugat, O. Diard, E. Keim, B. Marini, H.-W. Viehrig, K. Wallin, PERFECT (prediction of irradiation damage effects in reactor components): overview of RPV mechanics subproject, in: Proceedings of 2005 ASME Pressure Vessels and Piping Conference, ASME, Denver, Colorado, USA, 2005 (paper 71558).
[17] M. Hernández-Mayoral, D. Gomez-Briceno, J. Nucl. Mater. 399 (2010) 146–153.
[18] E. Meslin, B. Radiguet, P. Pareige, A. Barbu, J. Nucl. Mater. 399 (2010) 137–145.
[19] M. Lambrecht, L. Malerba, A. Almazouzi, J. Nucl. Mater. 378 (2008) 282–290.
[20] R.E. Stoller, in: ASTM STP 1447, ASTM International, West Conshohocken, PA, 2003. p. 326.
[21] G.R. Odette, T. Yamamoto, D. Klingensmith, Philos. Mag. 85 (2005) 779–797.
[22] F. Bergner, A. Ulbricht, H. Hein, M. Kammel, J. Phys.: Condens. Matter 20 (2008) 104262.
[23] M. Lambrecht, A. Almazouzi, J. Nucl. Mater. 385 (2009) 334–338.
[24] J. Kohlbrecher, W. Wagner, J. Appl. Cryst. 33 (2000) 804–806.
[25] M.H. Mathon, A. Barbu, F. Dunstetter, F. Maury, N. Lorenzelli, C.H. de Novion, J. Nucl. Mater. 245 (1997) 224–237.
[26] U. Keiderling, Appl. Phys. A 74 (Suppl.) (2002) S1455.
[27] O. Glatter, J. Appl. Cryst. 13 (1980) 7–11.
[28] G. Solt, F. Frisius, W.B. Waeber, P. Tipping, in: Effects of Radiation on Materials: 16th Int. Symp., ASTM STP 1175, ASTM, Philadelphia, 1993, p. 444.
[29] F. Bergner, A. Almazouzi, M. Hernandez-Mayoral, A. Ulbricht, Combined TEM PAS and SANS investigation of neutron-irradiated pure iron, OECD Handbook: Nuclear Science "Structural Materials for Innovative Nuclear Systems (SMINS)", 2008, pp. 283–290.
[30] F. Bergner, A. Ulbricht, M. Hernandez-Mayoral, P.K. Pranzas, J. Nucl. Mater. 374 (2008) 334–337.
[31] A. Ulbricht, J. Böhmert, H.-W. Viehrig, Journal of ASTM International 2 (2005) JAI12385.
[32] A. Ulbricht, F. Bergner, C.D. Dewhurst, A. Heinemann, J. Nucl. Mater. 353 (2006) 27–34.
[33] F. Bergner, A. Ulbricht, A. Gokhman, D. Erak, J. Nucl. Mater. 373 (2008) 199–205.
[34] P. Pareige, B. Radiguet, A. Barbu, J. Nucl. Mater. 352 (2006) 75–79.
[35] B. Radiguet, A. Barbu, P. Pareige, J. Nucl. Mater. 360 (2007) 104–117.
[36] Q. Xu, T. Yoshiie, K. Sato, Phys. Rev. B 73 (2006) 134115.